Computers and Fluids 179 (2019) 422–436

Contents lists available at ScienceDirect

Computers and Fluids

journal homepage: www.elsevier.com/locate/compfluid

A new hybrid WENO scheme for hyperbolic conservation laws

Zhuang Zhao[a], Jun Zhu[b], Yibing Chen[c], Jianxian Qiu[d,*]

[a] School of Mathematical Sciences, Xiamen University, Xiamen, Fujian, 361005, P.R. China
[b] College of Science, Nanjing University of Aeronautics and Astronautics, Nanjing, Jiangsu, 210016, P.R. China
[c] Institute of Applied Physics and Computational Mathematics, Beijing, 100094, China
[d] School of Mathematical Sciences and Fujian Provincial Key Laboratory of Mathematical Modeling and High-Performance Scientific Computing, Xiamen University, Xiamen, Fujian, 361005, P.R. China

ARTICLE INFO

Article history:
Received 9 June 2018
Revised 29 September 2018
Accepted 5 October 2018
Available online 20 November 2018

MSC:
65M60
35L65

Keywords:
WENO Scheme
Hyperbolic conservation laws
Hybrid
Finite difference framework

ABSTRACT

In [28], a simple fifth order weighted essentially non-oscillatory (WENO) scheme was presented in the finite difference framework for the hyperbolic conservation laws, in which the reconstruction of fluxes is a convex combination of a fourth degree polynomial with two linear polynomials. In this follow-up paper, we propose a new fifth order hybrid weighted essentially non-oscillatory (WENO) scheme based on the simple WENO. The main idea of the hybrid WENO scheme is that if all extreme points of the reconstruction polynomial for numerical flux in the big stencil are located outside of the big stencil, then we reconstruct the numerical flux by upwind linear approximation directly, otherwise use the simple WENO procedure. Compared with the simple WENO, the major advantage is its higher efficiency with less numerical errors in smooth regions and less computational costs. Likewise, the hybrid WENO scheme still keeps the simplicity and robustness of the simple WENO scheme. Extensive numerical results for both one and two dimensional equations are performed to verify these good performance of the proposed scheme.

© 2018 Elsevier Ltd. All rights reserved.

1. Introduction

In this paper, we propose a hybrid weighted essentially non-oscillatory (WENO) scheme in the finite difference framework. This work can be regarded as a combination of the simple WENO scheme [28] and the modified WENO scheme [29] for solving hyperbolic conservation laws. The hybrid WENO scheme in this paper is easy to implement and costs less CPU time than the simple WENO scheme [28], which can also be utilized to simulate the rather extreme test cases such as the Sedov blast wave problem, the Leblanc problem and the high Mach number astrophysical jet problem, etc., with normal CFL number, without any additional positivity preserving procedure.

Recently, many successful numerical schemes have been applied for hyperbolic conservation laws. Among them, the finite difference or finite volume essentially non-oscillatory (ENO) and WENO schemes are widely used for nonlinear hyperbolic conservation laws which often contain shock, contact discontinuities and sophisticated smooth structures in fairly localized regions. It is well known that a good numerical method should obtain high order accuracy in smooth regions and avoid spurious oscillations nearby discontinuities simultaneously. Hence, Harten and Osher [8] gave a weaker version of the total variation diminishing (TVD) criterion [7] and on which they established a framework for the reconstruction of high order ENO type schemes. Then, Harten et al. [10] developed the finite volume ENO schemes to solve one dimensional problems, which gave the most important thought of ENO schemes by using an adaptive stencil based on the local smoothness. Therefore, ENO schemes can maintain high-order accuracy as the function is smooth, while avoid the Gibbs phenomena at discontinuities simultaneously. Next, Shu and Osher proposed a class finite difference ENO schemes [24,25]. Then, Liu, Osher and Chan [18] constructed the first WENO scheme mainly based on ENO scheme, which used a nonlinear convex combination of all the candidate stencils, and it was a third-order finite volume method in one space dimension. In [16], the third and fifth-order finite difference WENO schemes in multi-space dimensions were proposed by Jiang and Shu, which gave a general framework to design the smoothness indicators and nonlinear weights. In general, WENO schemes have the ability to simulate the problems, which contain both strong discontinuities and sophisticated smooth structures. Likewise, these various finite difference and finite volume ENO and WENO schemes were presented in the

* Corresponding author.
E-mail addresses: zzhao@stu.xmu.edu.cn (Z. Zhao), zhujun@nuaa.edu.cn (J. Zhu), chen_yibing@iapcm.ac.cn (Y. Chen), jxqiu@xmu.edu.cn (J. Qiu).

https://doi.org/10.1016/j.compfluid.2018.10.024
0045-7930/© 2018 Elsevier Ltd. All rights reserved.

literature [2,3,9,11,16,18,24,25,27] working well for these complex problems.

A key idea of WENO schemes is a linear combination of lower order numerical fluxes or reconstruction to obtain a higher order approximation, and for the system cases, the WENO schemes are based on local characteristic decomposition method to avoid spurious oscillations. However, the cost of computing the nonlinear weights and local characteristic decompositions is very high. To overcome these drawbacks, Jiang and Shu [16] computed the nonlinear weights from pressure and entropy instead of the characteristic values for hyperbolic conservations laws. Pirozzoli [21] developed an efficient hybrid compact-WENO scheme, which selected compact up-wind schemes to treat smooth regions, while chose WENO schemes to handle discontinuities regions. Hill and Pullin [12] developed a hybrid scheme combing the tuned center-difference schemes with WENO schemes, to expect the nonlinear weights would be achieved automatically in smooth regions away from shocks, but a switching principle was still necessary. Then, Li and Qiu [20] constructed the hybrid WENO schemes using different switching principles with Runge-Kutta time discretization, while Huang and Qiu [15] used the Lax-Wendroff time discretization procedure to design the hybrid WENO scheme. They both selected the different troubled-cell indicators listed by Qiu and Shu [22] from discontinuous Galerkin (DG) schemes, which identified the discontinuity, then reconstructed the numerical flux by upwind linear approximation in smooth regions and WENO approximation in discontinuous regions. However, different troubled-cell indicators may have different effects for the hybrid WENO scheme, moreover, many troubled-cell indicators need to adjust parameters for different problems to keep better non-oscillations near discontinuous and less computational cost. Hence, Zhu and Qiu [29] chose a new simple switching principle, which was just to use different reconstruction method by identifying the locations of all extreme points of the big reconstruction polynomial for numerical flux, and we will adopt this new methodology in this paper. Though the classical WENO schemes proposed by Jiang and Shu [16] work well for hyperbolic conversation laws, the linear weights have to rely on the specific points and meshes, furthermore, the linear weights may be negative or not exist in some cases for finite volume version on unstructured meshes. Therefore, Zhu and Qiu [28] presented a new simple WENO scheme in the finite difference framework, which had a convex combination of a fourth degree polynomial and other two linear polynomials by using any linear weights (the sum is equal to one), and they also extended this method to rectangular meshes [30], triangular meshes [32] and tetrahedral meshes [31] in finite volume framework. These finite difference and finite volume methods illustrate the simplicity, efficiency and robustness of the simple WENO scheme simultaneously. In this paper, we propose the fifth order hybrid WENO scheme in the finite difference framework for solving the hyperbolic conservation laws in one and two dimensions, and we choose the simple WENO method [28] as the WENO procedure. Compared with the simple WENO scheme, the hybrid WENO scheme is more efficient with less numerical errors in smooth regions and less computational costs. The hybrid WENO scheme still keeps the simplicity and robustness of the simple WENO method. The WENO procedure of these two schemes seeks out a smaller TVD-like stencil, hence, these two schemes would operate like a TVD scheme with a Albada-like limiter, which makes them closer to a monotonicity preserving scheme, so these two schemes have the ability to simulate some extreme examples, such as the Sedov blast wave, the Leblanc and the high Mach number astrophysical jet problems et al. using CFL number as usual and without any additional positivity preserving procedure. The main procedures of the hybrid WENO scheme are given as follows, at first, we reconstruct the quartic polynomial based on the nodal point information of the big spatial stencil, and identify the locations of all extreme points of the reconstruction polynomial for numerical flux. If all of the extreme points are outside of the big stencil, then reconstruct the numerical flux by upwind linear approximation straightforwardly, otherwise choose the simple WENO procedure [28]. The numerical results in Section 3 and [29] show that the quartic polynomial has at least one extreme point inside the big stencil near discontinuous regions, and the reconstruction of numerical flux is switched to the simple WENO procedure, the methods work well for all test cases in Section 3 and [29]. For the system cases, WENO reconstruction is based on local characteristic decompositions and flux splitting to avoid spurious oscillations just like the classical WENO schemes [16]. From the procedures of the hybrid WENO scheme as mentioned above, the scheme saves CPU time for reducing the computations of smoothness indicators, nonlinear weights and local characteristic decompositions by using the linear upwind approximation in smooth regions. The hybrid WENO scheme also has the advantage of less numerical errors in smooth regions, for the linear upwind approximation has higher accuracy than the WENO procedure. In short, the hybrid WENO scheme still keeps the robustness of the simple WENO scheme [28], while it is very easy to implement in practice and has higher efficiency.

The organization of the paper is as follows: in Section 2, we present the detailed procedures of the finite difference hybrid WENO scheme. In Section 3, some benchmark numerical tests are presented to illustrate the numerical accuracy, efficiency and robustness of the new hybrid WENO scheme. Concluding remarks are given in Section 4.

2. Hybrid WENO scheme

We consider one dimensional scalar hyperbolic conservation laws

$$\begin{cases} u_t + f_x(u) = 0, \\ u(x,0) = u_0(x). \end{cases} \tag{2.1}$$

The semi-discrete finite difference scheme of (2.1) is

$$\frac{du_i(t)}{dt} = L(u)_i, \tag{2.2}$$

where $u_i(t)$ is the numerical approximation to the point value of $u(x_i, t)$ and $L(u)_i$ is the fifth order spatial discrete formulation of $-f_x(u)$ at the target point x_i. The spatial domain is divided with uniform grid points $\{x_i\}$, with $x_{i+1} - x_i = h$, $x_{i+1/2} = x_i + h/2$, and the cells are denoted by $I_i = [x_{i-1/2}, x_{i+1/2}]$, then, the right hand side of (2.2) can be written as

$$L(u)_i = -\frac{1}{h}(\hat{f}_{i+1/2} - \hat{f}_{i-1/2}). \tag{2.3}$$

Here $\hat{f}_{i+1/2}$ is a numerical flux which is a fifth order approximation of $v_{i+1/2} = v(x_{i+1/2})$, where $v(x)$ is defined implicitly as in [16]:

$$f(u(x)) = \frac{1}{h}\int_{x-h/2}^{x+h/2} v(x)dx. \tag{2.4}$$

To keep the stability in the finite difference framework, we need to split the flux $f(u)$ into two parts: $f(u) = f^+(u) + f^-(u)$, where $\frac{df^+(u)}{du} \geq 0$ and $\frac{df^-(u)}{du} \leq 0$. Here, a globe Lax-Friedrichs flux splitting method is applied as

$$f^{\pm}(u) = \frac{1}{2}(f(u) \pm \alpha u), \tag{2.5}$$

in which α is taken as $\max_u |f'(u)|$ over the whole relevant range of u.

In the step 1 to 3, we will only introduce the reconstruction procedure of numerical flux $\hat{f}^+_{i+1/2}$ in detail, which is the fifth order approximation of the positive part of flux $f(u)$ at $x = x_{i+1/2}$,

while the formulas for the negative part of numerical flux $\hat{f}^-_{i+1/2}$ are mirror symmetric with respect to $x_{i+1/2}$ of that for $\hat{f}^+_{i+1/2}$ and will not be presented again, then the numerical flux $\hat{f}_{i+1/2}$ is set as $\hat{f}^+_{i+1/2}+\hat{f}^-_{i+1/2}$. In the step 4, the semi-discrete scheme (2.2) is then discretized by a fourth order Runge-Kutta method [24], when we have finished the spatial discretization by using the step 1 to 3.

Step 1. We choose the following big stencil: $T_0=\{I_{i-2},\dots,I_{i+2}\}$, then reconstruct the fourth degree polynomial $p_0(x)$ based on the nodal point information of the positive part of flux $f^+(u)$ as

$$\frac{1}{h}\int_{I_j} p_0(x)dx = f^+(u_j),\ \ j=i-2,\dots,i+2. \tag{2.6}$$

Let $\xi=\frac{(x-x_i)}{h}$, then we have the polynomial $p_0(x)$:

$$\begin{aligned} p_0(x) &= \frac{1}{1920}[(-116f^+_{i-1}+9f^+_{i-2}+2134f^+_i-116f^+_{i+1}+9f^+_{i+2}) \\ &\quad -40(34f^+_{i-1}-5f^+_{i-2}-34f^+_{i+1}+5f^+_{i+2})\xi+120(12f^+_{i-1} \\ &\quad -f^+_{i-2}-22f^+_i+12f^+_{i+1}-f^+_{i+2})\xi^2+160(2f^+_{i-1}-f^+_{i-2}-2f^+_{i+1} \\ &\quad +f^+_{i+2})\xi^3-80(4f^+_{i-1}-f^+_{i-2}-6f^+_i+4f^+_{i+1}-f^+_{i+2})\xi^4)], \end{aligned} \tag{2.7}$$

and its first derivative polynomial $p_0'(x)$ is

$$\begin{aligned} p_0'(x)=&\frac{1}{48h}[(-34f^+_{i-1}+5f^+_{i-2}+34f^+_{i+1}-5f^+_{i+2})+6(12f^+_{i-1}-f^+_{i-2} \\ &-22f^+_i+12f^+_{i+1}-f^+_{i+2})\xi+12(2f^+_{i-1}-f^+_{i-2}-2f^+_{i+1}+f^+_{i+2})\xi^2 \\ &+8(-4f^+_{i-1}+f^+_{i-2}+6f^+_i-4f^+_{i+1}+f^+_{i+2})\xi^3)] \end{aligned} \tag{2.8}$$

Step 2. Determine the extreme points of the reconstruction polynomial $p_0(x)$. Firstly, we find the zero points of $p_0'(x)$, then identify whether these zero points of $p_0'(x)$ are extreme points of $p_0(x)$ or not. As the degree of $p_0'(x)$ is at most three, we can solve the real zero points of $p_0'(x)$ based on [5] easily, and the explicit solving steps are shown in Appendix A. One is the extreme point of $p_0(x)$ if and only if it is the real zero point and not doubled zero point of $p_0'(x)$.

Step 3. Identify the locations of all extreme points of the reconstruction polynomial $p_0(x)$ and choose different reconstruction procedure according to the locations of the extreme points. If all of the extreme points of the polynomial $p_0(x)$ are outside of the big spatial stencil T_0, or the polynomial $p_0(x)$ doesn't have the extreme point, we take the final reconstruction of the numerical flux $\hat{f}^+_{i+1/2}$ as $p_0(x_{i+1/2})$ directly, otherwise, there is at least one of the extreme points of the reconstruction polynomial $p_0(x)$ inside the big spatial stencil T_0, then reconstruct the numerical flux $\hat{f}^+_{i+1/2}$ by using the simple and efficient WENO method [28] to avoid spurious oscillations, and we will review this simple and efficient WENO method in the following procedures. At first, we choose two smaller stencils $T_1=\{I_{i-1},I_i\}$ and $T_2=\{I_i,I_{i+1}\}$, then construct two polynomials $p_1(x)$ and $p_2(x)$ according to the nodal point information of the positive flux $f^+(u)$ on the stencils T_1 and T_2 respectively. Similarly as specified in step 1, it is easy to obtain the two smaller reconstructed polynomials satisfying

$$\frac{1}{h}\int_{I_j} p_1(x)dx = f^+(u_j),\ \ j=i-1,i, \tag{2.9}$$

and

$$\frac{1}{h}\int_{I_j} p_2(x)dx = f^+(u_j),\ \ j=i,i+1. \tag{2.10}$$

Their explicit expressions are

$$p_1(x)=f^+_i+(f^+_i-f^+_{i-1})\left(\frac{x-x_i}{h}\right), \tag{2.11}$$

and

$$p_2(x)=f^+_i+(f^+_{i+1}-f^+_i)\left(\frac{x-x_i}{h}\right). \tag{2.12}$$

In this paper, we take the linear weights are $\gamma_0=0.8$, $\gamma_1=0.1$ and $\gamma_2=0.1$ for all test cases, as the random choice of the linear weights would not pollute the optimal order accuracy of the simple WENO scheme, then, we compute the smoothness indicators β_l, which measure how smooth the functions $p_l(x)$ are in the target cell I_i, and we use the same definition for the smoothness indicators as in [2,16,26]

$$\beta_l=\sum_{\alpha=1}^{r}\int_{I_i} h^{2\alpha-1}\left(\frac{d^\alpha p_l(x)}{dx^\alpha}\right)^2 dx. \tag{2.13}$$

The explicit expressions are shown respectively,

$$\begin{aligned} \beta_0 =& \frac{(f^+_{i-2}-8f^+_{i-1}+8f^+_{i+1}-f^+_{i+2})^2}{144} \\ &+\frac{781(-f^+_{i-2}+2f^+_{i-1}-2f^+_{i+1}+f^+_{i+2})^2}{2880} \\ &+\frac{(-11f^+_{i-2}+174f^+_{i-1}-326f^+_i+174f^+_{i+1}-11f^+_{i+2})^2}{15600} \\ &+\frac{1421461(f^+_{i-2}-4f^+_{i-1}+6f^+_i-4f^+_{i+1}+f^+_{i+2})^2}{1310400}, \end{aligned} \tag{2.14}$$

$$\beta_1=(f^+_{i-1}-f^+_i)^2, \tag{2.15}$$

and

$$\beta_2=(f^+_i-f^+_{i+1})^2. \tag{2.16}$$

Then we take a new parameter τ to measure the absolute deference between β_0, β_1 and β_2, which is different to the formula set in [1,4],

$$\tau=\left(\frac{|\beta_0-\beta_1|+|\beta_0-\beta_2|}{2}\right)^2, \tag{2.17}$$

and the nonlinear weights are formulated as

$$\omega_n=\frac{\bar{\omega}_n}{\sum_{\ell=0}^{2}\bar{\omega}_\ell},\ \text{with}\ \bar{\omega}_n=\gamma_n\left(1+\frac{\tau}{\varepsilon+\beta_n}\right),\ \ n=0,1,2. \tag{2.18}$$

Here ε is a small positive number to avoid the denominator by zero, and we take $\varepsilon=10^{-6}$ in our computation as usual. Hence, the final reconstruction of the numerical flux $f^+(u)$ at $x=x_{i+1/2}$ is given by

$$\begin{aligned} \hat{f}^+_{i+1/2} =& \omega_0\left(\frac{1}{\gamma_0}p_0(x_{i+1/2})-\frac{\gamma_1}{\gamma_0}p_1(x_{i+1/2})-\frac{\gamma_2}{\gamma_0}p_2(x_{i+1/2})\right) \\ &+\omega_1 p_1(x_{i+1/2})+\omega_2 p_2(x_{i+1/2}). \end{aligned} \tag{2.19}$$

Step 4. The semi-discrete scheme (2.2) is discretized in time by a fourth order Runge-Kutta method [24]

$$\begin{cases} u^{(1)} &= u^n+\frac{1}{2}\Delta tL(u^n), \\ u^{(2)} &= u^n+\frac{1}{2}\Delta tL(u^{(1)}), \\ u^{(3)} &= u^n+\Delta tL(u^{(2)}), \\ u^{n+1} &= -\frac{1}{3}u^n+\frac{1}{3}u^{(1)}+\frac{2}{3}u^{(2)}+\frac{1}{3}u^{(3)}+\frac{1}{6}\Delta tL(u^{(3)}). \end{cases} \tag{2.20}$$

Remark: For the system cases, such as the compressible Euler equations, all of the WENO reconstruction procedure is implemented with a local characteristic field decomposition listed by [16], while the upwind linear approximation is performed by component by component. For the two dimensional cases, the reconstruction for numerical fluxes is constructed by dimension by dimension.

Table 3.1
Computing time of numerical examples: the total CPU time of example 3.1 to 3.11 for the hybrid WENO scheme and the simple WENO scheme; the ratios of the total CPU time by the hybrid WENO scheme over the simple WENO scheme on the same numerical example.

Numerical example	CPU time of hybrid WENO scheme(S)	CPU time of simple WENO scheme (S)	Ratio
3.1 $\rho(x,0)=1+0.99\sin(x)$	13222.0	18979.2	69.7%
3.1 $\rho(x,0)=1+0.999\sin(x)$	38623.3	56730.0	68.1%
3.1 $\rho(x,0)=1+0.99999\sin(x)$	295441.2	442528.6	66.7%
3.2 $\rho(x,y,0)=1+0.99\sin(x+y)$	7323.03	11864.8	61.7%
3.2 $\rho(x,y,0)=1+0.999\sin(x+y)$	22758.2	33925.9	67.1%
3.2 $\rho(x,y,0)=1+0.99999\sin(x+y)$	205910.3	309802.6	66.5%
3.3 Lax problem	0.04680	0.09360	50.0%
3.4 Shu-Osher problem	0.3120	0.4836	64.5%
3.5 Two blast waves	2.0904	3.3384	62.6%
3.6 1D sedov blast wave	0.5772	0.6240	92.5%
3.7 Double rarefaction wave	0.1092	0.2184	50.0%
3.8 Leblanc problem	51.4803	79.5449	64.7%
3.9 Double Mach reflection	13980.0	18208.2	76.8%
3.10 2D sedov blast wave	454.766	585.919	77.6%
3.11 80 Mach astrophysical jet	785.785	916.224	85.8%
3.11 2000 Mach astrophysical jet	1861.49	2133.82	87.2%

Table 3.2
1D-Euler equations: initial data $\rho(x,0)=1+0.99\sin(x)$, $\mu(x,0)=1$ and $p(x,0)=1$. Hybrid WENO and Simple WENO schemes. $T=0.1$. L^1 and L^∞ errors.

grid points	Hybrid WENO scheme				Simple WENO scheme			
	L^1 error	order	L^∞error	order	L^1 error	order	L^∞ error	order
40	7.167E-04		4.540E-03		7.841E-04		5.045E-03	
80	9.877E-06	6.18	8.962E-05	5.66	9.764E-06	6.33	8.973E-05	5.81
160	5.729E-08	7.43	1.232E-06	6.18	5.488E-08	7.47	1.241E-06	6.18
320	2.150E-10	8.06	6.018E-09	7.68	1.913E-10	8.16	6.384E-09	7.60
640	1.350E-12	7.32	2.124E-12	11.47	1.658E-12	6.85	3.477E-11	7.52
1280	4.223E-14	5.00	6.637E-14	5.00	4.223E-14	5.30	1.643E-13	7.73
2560	1.320E-15	5.00	2.074E-15	5.00	1.320E-15	5.00	2.287E-15	6.17
5120	4.126E-17	5.00	6.482E-17	5.00	4.126E-17	5.00	6.510E-17	5.13
10,240	1.289E-18	4.99	2.026E-18	4.99	1.289E-18	4.99	2.026E-18	5.00
20,480	4.030E-20	5.00	6.330E-20	5.00	4.030E-20	5.00	6.330E-20	5.00

3. Numerical tests

In this section, we perform the results and the total CPU time of numerical tests of the hybrid WENO scheme which is outlined in the previous section comparing with the simple WENO scheme [28]. The CFL number is set as 0.6 for these two schemes as usual. Simple WENO and Hybrid WENO are termed as the two schemes respectively. Since the random choice of the linear weights would not pollute the optimal order accuracy of the simple WENO scheme, we take γ_0=0.8, γ_1=0.1 and γ_2=0.1 for all numerical tests.

At the first, we list the CPU time for all test cases to show that the hybrid WENO scheme costs less CPU time than simple WENO. In the Table 3.1, we present the total cpu time for all test cases by the hybrid WENO scheme and the simple WENO scheme. Compared with the simple WENO scheme, the hybrid WENO scheme may almost save 50% CPU time in one dimensional problems and save 40% CPU time in two dimensional problems, when the numerical examples have many smooth regions, but in some extreme numerical example, like the Sedov blast wave problem and the high Mach number astrophysical jet problem, the hybrid WENO scheme may only save 15% CPU time. In short, the hybrid WENO scheme uses less CPU time than the simple WENO scheme in the same numerical test.

Example 3.1.

$$\frac{\partial}{\partial t}\begin{pmatrix}\rho\\ \rho\mu\\ E\end{pmatrix}+\frac{\partial}{\partial x}\begin{pmatrix}\rho\mu\\ \rho\mu^2+p\\ \mu(E+p)\end{pmatrix}=0. \tag{3.1}$$

Here ρ is density, μ is the velocity, E is total energy and p is pressure. The initial conditions are set to be (1) $\rho(x,0)=1+0.99\sin(x)$; (2) $\rho(x,0)=1+0.999\sin(x)$; (3) $\rho(x,0)=1+0.99999\sin(x)$; and $\mu(x,0)=1$, $p(x,0)=1$, $\gamma=1.4$. The computing domain is $x\in[0,\ 2\pi]$, with a periodic boundary condition. The exact solutions are: (1) $\rho(x,t)=1+0.99\sin(x-t)$; (2) $\rho(x,t)=1+0.999\sin(x-t)$; (3) $\rho(x,t)=1+0.99999\sin(x-t)$, respectively. We compute the solution up to $T=0.1$. The numerical errors and orders of the density for the hybrid WENO scheme and the simple WENO scheme are shown in Table 3.2, Table 3.3 and Table 3.4, respectively. From these tables, we can see the numerical errors of the hybrid WENO scheme are smaller than the simple WENO on the same meshes. Usually, we only can obtain the designed accuracy order when meshes are small enough. We find that both two schemes finally achieve the designed fifth order for case (1) and (2) in Table 3.2 and Table 3.3, respectively, when the meshes are small enough. In Table 3.4, the hybrid WENO scheme achieve the fifth order on 10,240 and 20,480 grid points, while the simple WENO scheme exceed the designed fifth order for case (3). In Fig. 3.1, Fig. 3.2 and Fig. 3.3, we show numerical errors against CPU times by using the hybrid WENO scheme and the simple WENO scheme for case (1), (2) and (3), which illustrate the hybrid WENO scheme uses less CPU times and has smaller numerical errors than the simple WENO scheme on the same meshes. In Table 3.1, compared with the simple WENO scheme, the hybrid WENO scheme saves almost 30% CPU time with different initial conditions in this numerical example. Hence, the hybrid WENO scheme is more efficient than the simple WENO scheme in this one dimensional benchmark test case with different extreme initial conditions.

Table 3.3
1D-Euler equations: initial data $\rho(x,0) = 1 + 0.999\sin(x)$, $\mu(x,0) = 1$ and $p(x,0) = 1$. Hybrid WENO and Simple WENO schemes. $T = 0.1$. L^1 and L^∞ errors.

grid points	Hybrid WENO scheme				Simple WENO scheme			
	L^1 error	order	L^∞error	order	L^1 error	order	L^∞ error	order
40	1.243E-03		7.436E-03		1.215E-03		7.454E-03	
80	7.663E-05	4.02	6.042E-04	3.62	7.563E-05	4.01	6.071E-04	3.62
160	2.542E-06	4.91	4.979E-05	3.60	2.514E-06	4.91	5.020E-05	3.60
320	9.815E-09	8.02	2.778E-07	7.49	1.002E-08	7.97	2.937E-07	7.42
640	4.188E-11	7.87	1.886E-09	7.20	4.908E-11	7.67	2.429E-09	6.92
1280	1.275E-13	8.36	2.004E-13	13.20	3.113E-13	7.30	1.560E-11	7.28
2560	3.988E-15	5.00	6.266E-15	5.00	4.019E-15	6.28	5.132E-14	8.25
5120	1.246E-16	5.00	1.958E-16	5.00	1.246E-16	5.01	2.964E-16	7.44
10,240	3.896E-18	5.00	6.120E-18	5.00	3.896E-18	5.00	6.307E-18	5.55
20,480	1.217E-19	5.00	1.912E-19	5.00	1.217E-19	5.00	1.913E-19	5.04

Table 3.4
1D-Euler equations: initial data $\rho(x,0) = 1 + 0.99999\sin(x)$, $\mu(x,0) = 1$ and $p(x,0) = 1$. Hybrid WENO and Simple WENO schemes. $T = 0.1$. L^1 and L^∞ errors.

grid points	Hybrid WENO scheme				Simple WENO scheme			
	L^1 error	order	L^∞error	order	L^1 error	order	L^∞ error	order
40	1.368E-03		8.025E-03		1.330E-03		8.055E-03	
80	1.221E-04	3.49	9.432E-04	3.09	1.213E-04	3.46	9.600E-04	3.07
160	1.549E-05	2.98	2.758E-04	1.77	1.531E-05	2.99	2.810E-04	1.77
320	1.178E-06	3.72	2.399E-05	3.52	1.226E-06	3.64	2.589E-05	3.44
640	4.537E-08	4.70	1.581E-06	3.92	5.274E-08	4.54	1.862E-06	3.80
1280	4.206E-10	6.75	2.647E-08	5.90	6.241E-10	6.40	3.910E-08	5.57
2560	1.845E-12	7.83	1.996E-10	7.05	5.361E-12	6.86	5.560E-10	6.14
5120	1.215E-15	10.57	1.908E-15	16.67	3.570E-14	7.23	4.900E-12	6.83
10,240	3.805E-17	5.00	5.978E-17	5.00	1.591E-16	7.81	1.433E-14	8.42
20,480	1.190E-18	4.99	1.869E-18	4.99	1.340E-18	6.88	3.596E-17	8.64

Table 3.5
2D-Euler equations: initial data $\rho(x,y,0) = 1 + 0.99\sin(x+y)$, $\mu(x,y,0) = 1$, $v(x,y,0) = 1$ and $p(x,y,0) = 1$. Hybrid WENO and Simple WENO schemes. $T = 0.1$. L^1 and L^∞ errors.

grid points	Hybrid WENO scheme				Simple WENO scheme			
	L^1 error	order	L^∞error	order	L^1 error	order	L^∞ error	order
40×40	6.06E-04		2.86E-03		6.69E-04		3.19E-03	
80×80	2.65E-05	4.51	3.08E-04	3.21	2.63E-05	4.67	3.09E-04	3.37
160×160	8.92E-08	8.22	1.46E-06	7.72	8.62E-08	8.26	1.48E-06	7.70
320×320	3.73E-10	7.90	9.24E-09	7.30	3.60E-10	7.90	1.03E-08	7.18
640×640	2.70E-12	7.11	4.25E-12	11.09	3.31E-12	6.77	6.54E-11	7.29
1280×1280	8.46E-14	5.00	1.48E-13	4.85	8.46E-14	5.29	3.27E-13	7.65

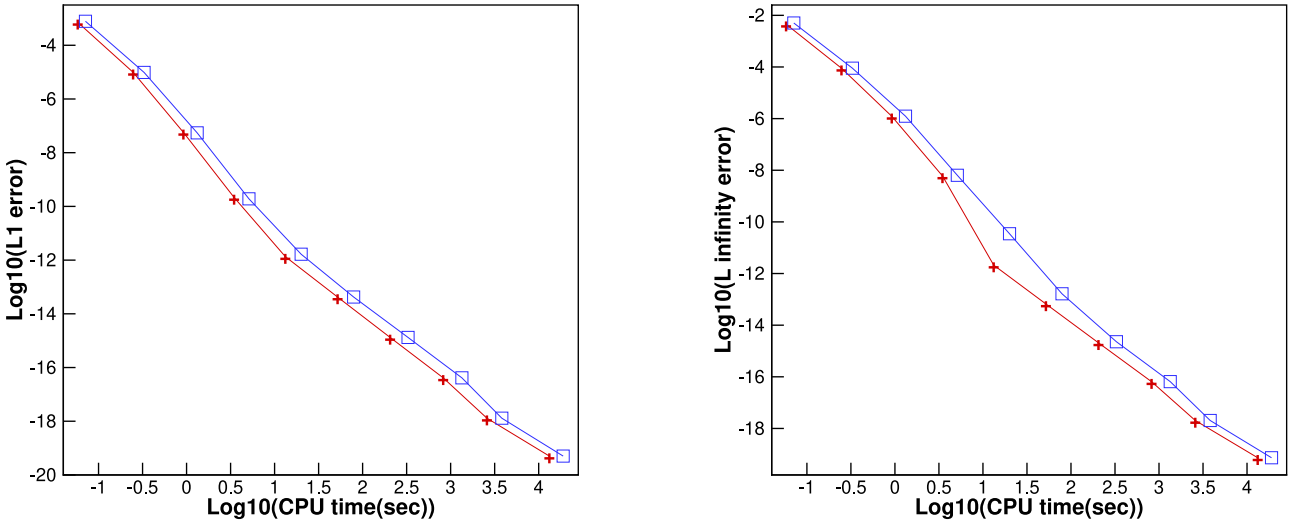

Fig. 3.1. 1D-Euler equations: initial data $\rho(x,0) = 1 + 0.99\sin(x)$, $\mu(x,0) = 1$ and $p(x,0) = 1$. $T = 0.1$. Computing time and error. Plus signs and a solid line denote the results of the hybrid WENO scheme; square and a solid line denote the results of the simple WENO scheme.

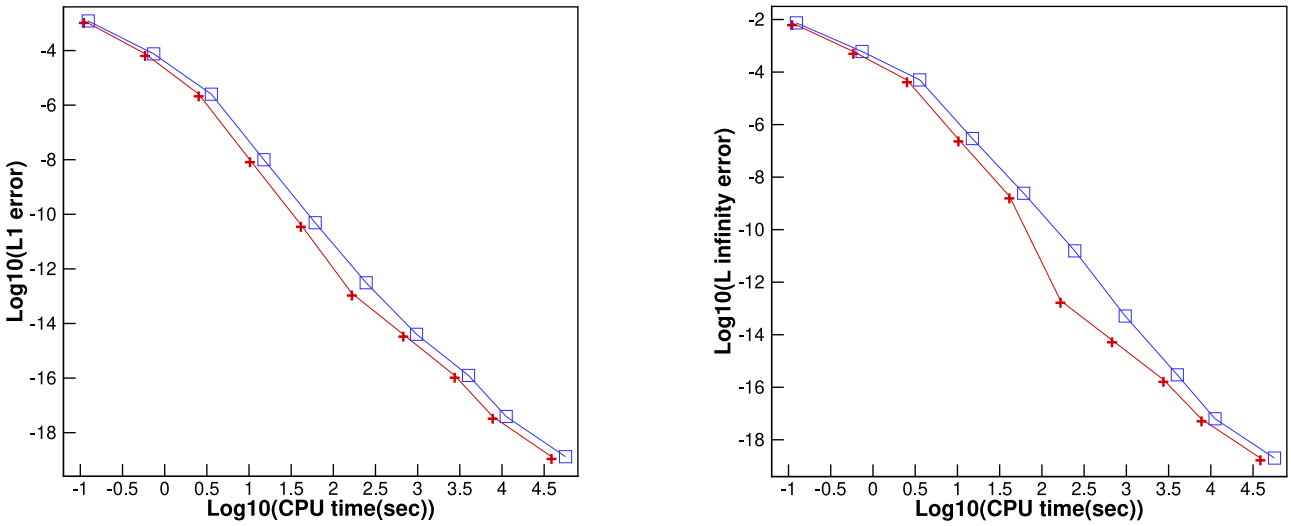

Fig. 3.2. 1D-Euler equations: initial data $\rho(x,0) = 1 + 0.999\sin(x)$, $\mu(x,0) = 1$ and $p(x,0) = 1$. $T = 0.1$. Computing time and error. Plus signs and a solid line denote the results of the hybrid WENO scheme; square and a solid line denote the results of the simple WENO scheme.

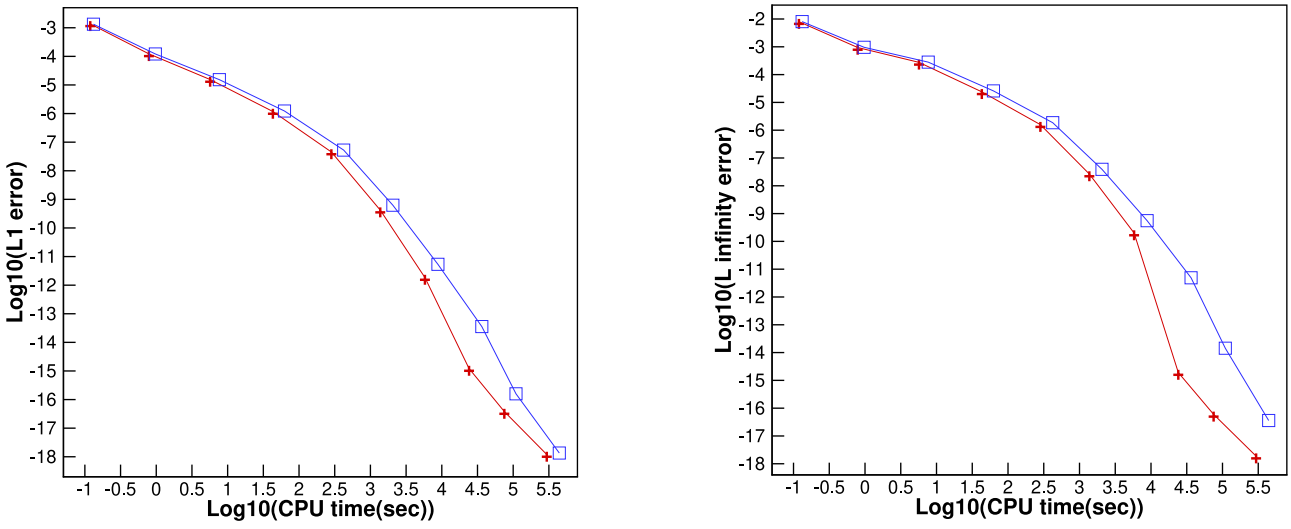

Fig. 3.3. 1D-Euler equations: initial data $\rho(x,0) = 1 + 0.99999\sin(x)$, $\mu(x,0) = 1$ and $p(x,0) = 1$. $T = 0.1$. Computing time and error. Plus signs and a solid line denote the results of the hybrid WENO scheme; square and a solid line denote the results of the simple WENO scheme.

Table 3.6
2D-Euler equations: initial data $\rho(x,y,0) = 1 + 0.999\sin(x+y)$, $\mu(x,y,0) = 1$, $\nu(x,y,0) = 1$ and $p(x,y,0) = 1$. Hybrid WENO and Simple WENO schemes. $T = 0.1$. L^1 and L^∞ errors.

grid points	Hybrid WENO scheme				Simple WENO scheme			
	L^1 error	order	L^∞error	order	L^1 error	order	L^∞ error	order
40×40	1.26E-03		5.61E-03		1.25E-03		5.68E-03	
80×80	1.57E-04	3.00	1.52E-03	1.89	1.56E-04	3.00	1.52E-03	1.90
160×160	3.23E-06	5.61	4.51E-05	5.07	3.24E-06	5.59	4.60E-05	5.05
320×320	1.66E-08	7.60	4.09E-07	6.78	1.75E-08	7.54	4.45E-07	6.69
640×640	7.08E-11	7.87	2.79E-09	7.20	9.04E-11	7.59	3.92E-09	6.83
1280×1280	2.55E-13	8.12	4.29E-13	12.67	6.18E-13	7.19	2.97E-11	7.04

Table 3.7
2D-Euler equations: initial data $\rho(x,y,0) = 1 + 0.99999\sin(x+y)$, $\mu(x,y,0) = 1$, $\nu(x,y,0) = 1$ and $p(x,y,0) = 1$. Hybrid WENO and Simple WENO schemes. $T = 0.1$. L^1 and L^∞ errors.

grid points	Hybrid WENO scheme				Simple WENO scheme			
	L^1 error	order	L^∞error	order	L^1 error	order	L^∞ error	order
40×40	1.41E-03		6.21E-03		1.40E-03		6.30E-03	
80×80	2.12E-04	2.73	1.96E-03	1.67	2.06E-04	2.76	1.98E-03	1.67
160×160	1.90E-05	3.48	2.21E-04	3.14	1.93E-05	3.42	2.31E-04	3.10
320×320	1.64E-06	3.53	3.04E-05	2.86	1.75E-06	3.47	3.32E-05	2.80
640×640	7.01E-08	4.55	2.22E-06	3.78	8.39E-08	4.38	2.68E-06	3.63
1280×1280	6.83E-10	6.68	3.90E-08	5.83	1.08E-09	6.28	6.15E-08	5.45

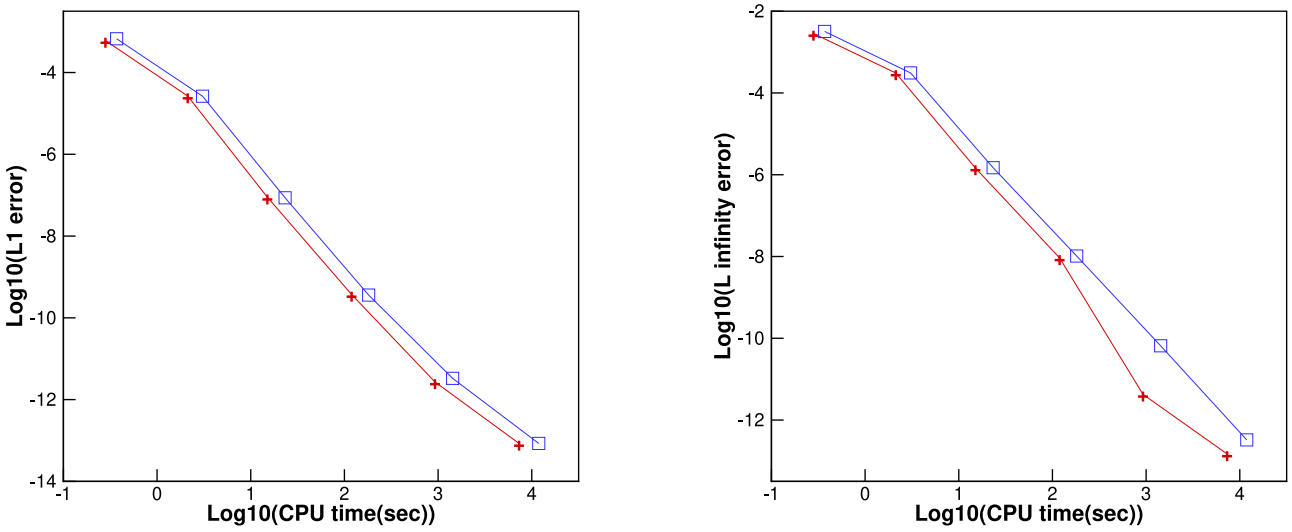

Fig. 3.4. 2D-Euler equations: initial data $\rho(x,y,0)=1+0.99\sin(x+y)$, $\mu(x,y,0)=1$, $\nu(x,y,0)=1$ and $p(x,y,0)=1$. $T=0.1$. Computing time and error. Plus signs and a solid line denote the results of the hybrid WENO scheme; square and a solid line denote the results of the simple WENO scheme.

Example 3.2.

$$\frac{\partial}{\partial t}\begin{pmatrix}\rho\\ \rho\mu\\ \rho\nu\\ E\end{pmatrix}+\frac{\partial}{\partial x}\begin{pmatrix}\rho\mu\\ \rho\mu^2+p\\ \rho\mu\nu\\ \mu(E+p)\end{pmatrix}+\frac{\partial}{\partial y}\begin{pmatrix}\rho\nu\\ \rho\mu\nu\\ \rho\nu^2+p\\ \nu(E+p)\end{pmatrix}=0. \tag{3.2}$$

In which ρ is density; μ and ν are the velocities in the x and y directions, respectively; E is total energy; and p is pressure. The initial conditions are: (1) $\rho(x,y,0)=1+0.99\sin(x+y)$; (2) $\rho(x,y,0)=1+0.999\sin(x+y)$; (3) $\rho(x,y,0)=1+0.99999\sin(x+y)$; and $\mu(x,y,0)=1$, $\nu(x,y,0)=1$, $p(x,y,0)=1$, $\gamma=1.4$. The computing domain is $(x,\ y)\in[0,\ 2\pi]\times[0,\ 2\pi]$, with a periodic boundary conditions in both directions. The final computing time is $T=0.1$. The numerical errors and orders of the density for the hybrid WENO scheme and the simple WENO schemes are shown in Table 3.5, Table 3.6 and Table 3.7, respectively. From these tables, we can know that the numerical errors of the hybrid WENO scheme are smaller than the simple WENO scheme on the same meshes. We also find these two schemes exceed the designed order in case (2) and (3) shown in Table 3.6 and Table 3.7, respectively, while these two scheme achieve fifth order accuracy for case (1) given in Table 3.5. As in the Example 3.1, we do think that both two schemes can achieve the designed fifth order when the meshes are small enough. In Fig. 3.4, Fig. 3.5 and Fig. 3.6, we show numerical errors against CPU times for case (1), (2) and (3) with different schemes, which illustrate the hybrid WENO scheme uses less CPU times and has smaller numerical errors in comparison with the simple WENO scheme on the same meshes, and we can see that in Table 3.1 as well. Therefore, the hybrid WENO scheme is more efficient than the simple WENO scheme in this two dimensional test case with three extreme density initial conditions.

Example 3.3. The Lax problem, and the initial condition is

$$(\rho,\mu,p,\gamma)^T=\begin{cases}(0.445,0.698,3.528,1.4)^T, & x\in[-0.5,0),\\ (0.5,0,0.571,1.4)^T, & x\in[0,0.5].\end{cases} \tag{3.3}$$

The final computing time is $T=0.16$, and we first compare the performances of the exact solution and the computed density ρ obtained with the hybrid WENO scheme and the simple WENO scheme by using 200 grid points in Fig. 3.7, then, the zoomed in picture for different schemes and the time history of the points where the simple WENO reconstruction procedure is used in the hybrid WENO scheme are also given in Fig. 3.7. These two schemes also have similar computational results, however, the hybrid WENO scheme saves almost 50% computational time which can be seen in Table 3.1.

Example 3.4. The Shu-Osher problem, which describes shock interaction with entropy waves [26], and the initial condition is

$$(\rho,\mu,p,\gamma)^T=\begin{cases}(3.857143,2.629369,10.333333,1.4)^T, & x\in[-5,-4),\\ (1+0.2\sin(5x),0,1,1.4)^T, & x\in[-4,5].\end{cases} \tag{3.4}$$

This is a typical problem with a moving Mach=3 shock interacting with sine waves in density, which means that the solution contains both shocks and complex smooth region structures, and the final time is $T=1.8$. In Fig. 3.8, we present the computed density ρ against the referenced "exact" solution, the zoomed in picture for different schemes and the time history of the points where the simple WENO reconstruction procedure is used in hybrid WENO scheme, and the referenced "exact" solution is computed by the fifth order finite difference WENO scheme [16] with 2000 grid points. Again, we all see that the computational results by the hybrid WENO scheme are similar to the simple WENO scheme, but we find the hybrid WENO scheme uses less CPU time from the Table 3.1.

Example 3.5. The interaction of two blast waves, and the initial conditions are:

$$(\rho,\mu,p,\gamma)^T=\begin{cases}(1,0,10^3,1.4)^T, & 0<x<0.1,\\ (1,0,10^{-2},1.4)^T, & 0.1<x<0.9,\\ (1,0,10^2,1.4)^T, & 0.9<x<1.\end{cases} \tag{3.5}$$

In Fig. 3.9, we show the computed density at the final time $T=0.038$ against the reference "exact" solution, the zoomed in picture for different schemes and the time history of the points by using the simple WENO reconstruction procedure in the hybrid WENO scheme. Again, the reference "exact" solution is a converged solution computed by the fifth order finite difference WENO scheme [16] with 2000 grid points. The computational results by these schemes are similar as well, and their CPU time are shown in Table 3.1 similarly as the hybrid WENO scheme saves near 40% CPU time.

Example 3.6. The Sedov blast wave problem, which contains very low density with strong shocks. The exact solution is specified in [17,23]. The computational domain is $[-2,2]$ and initial conditions are: $\rho=1$, $\mu=0$, $E=10^{-12}$ everywhere except that the energy is

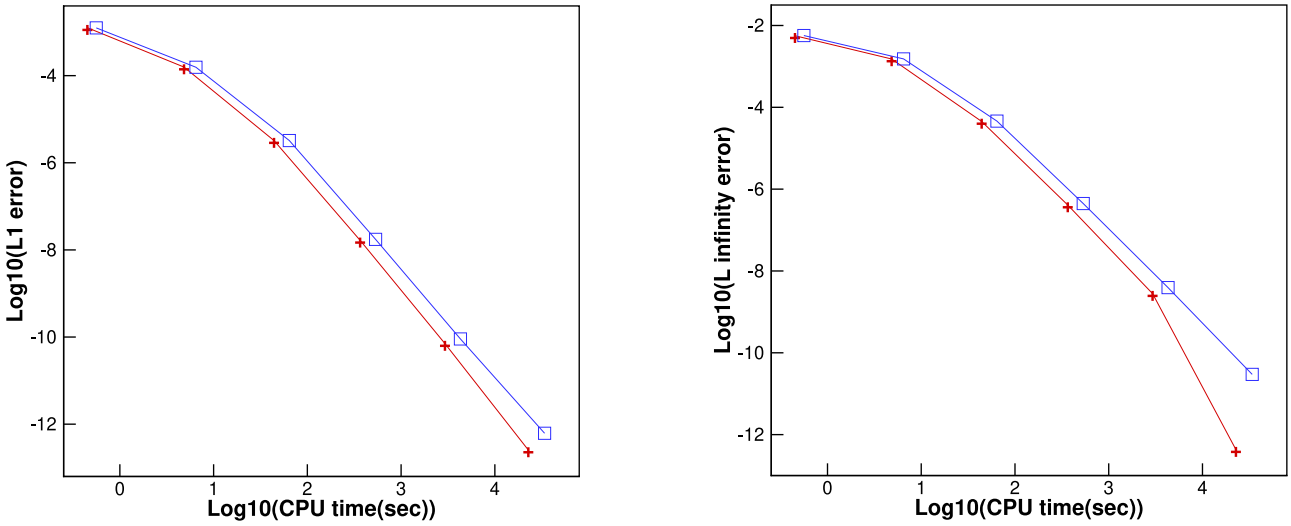

Fig. 3.5. 2D-Euler equations: initial data $\rho(x, y, 0) = 1 + 0.999\sin(x + y)$, $\mu(x, y, 0) = 1$, $v(x, y, 0) = 1$ and $p(x, y, 0) = 1$. $T = 0.1$. Computing time and error. Plus signs and a solid line denote the results of the hybrid WENO scheme; square and a solid line denote the results of the simple WENO scheme.

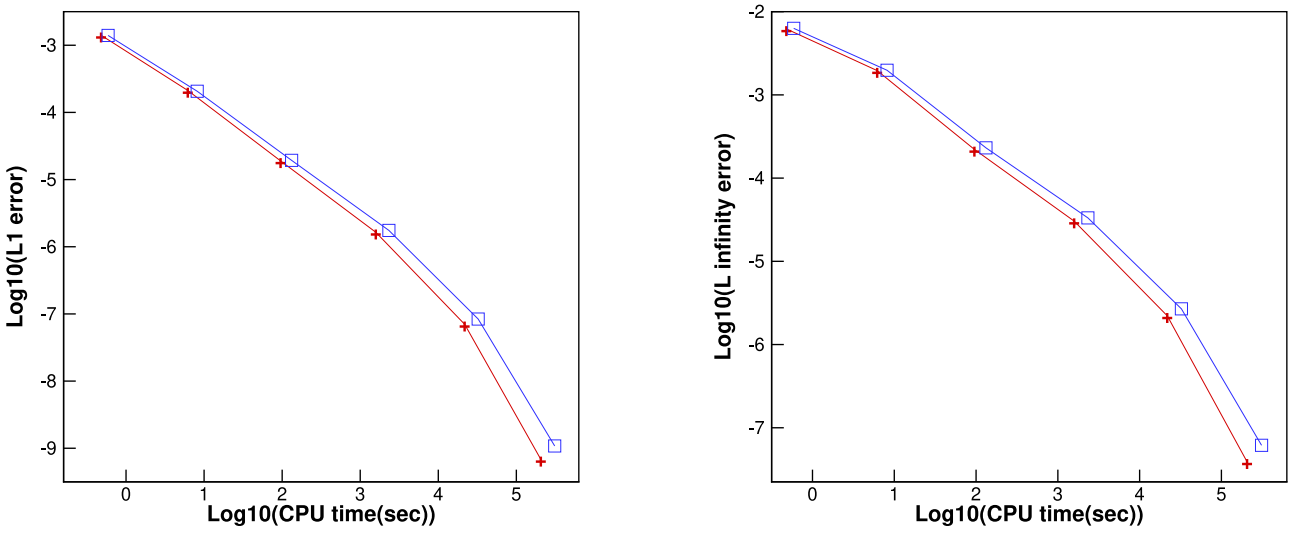

Fig. 3.6. 2D-Euler equations: initial data $\rho(x, y, 0) = 1 + 0.99999\sin(x + y)$, $\mu(x, y, 0) = 1$, $v(x, y, 0) = 1$ and $p(x, y, 0) = 1$. $T = 0.1$. Computing time and error. Plus signs and a solid line denote the results of the hybrid WENO scheme; square and a solid line denote the results of the simple WENO scheme.

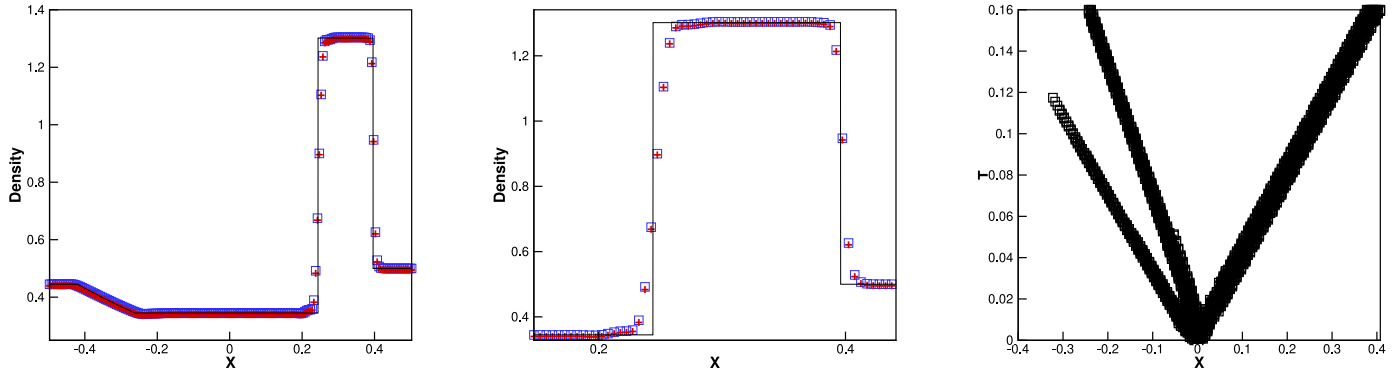

Fig. 3.7. The Lax problem. T=0.16. From left to right: density; density zoomed in; the points where the simple WENO reconstruction procedure is used in the hybrid WENO scheme. Solid line: the exact solution; plus signs: the results of the hybrid WENO scheme; squares: the results of the simple WENO scheme. Grid points: 200.

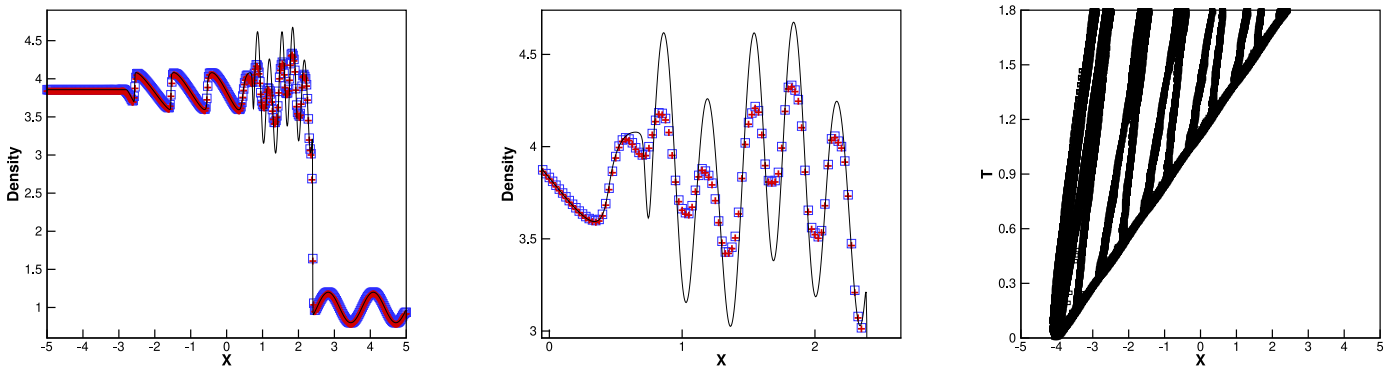

Fig. 3.8. The shock density wave interaction problem. T=1.8. From left to right: density; density zoomed in; the points where the simple WENO reconstruction procedure is used in the hybrid WENO scheme. Solid line: the exact solution; plus signs: the results of the hybrid WENO scheme; squares: the results of the simple WENO scheme. Grid points: 400.

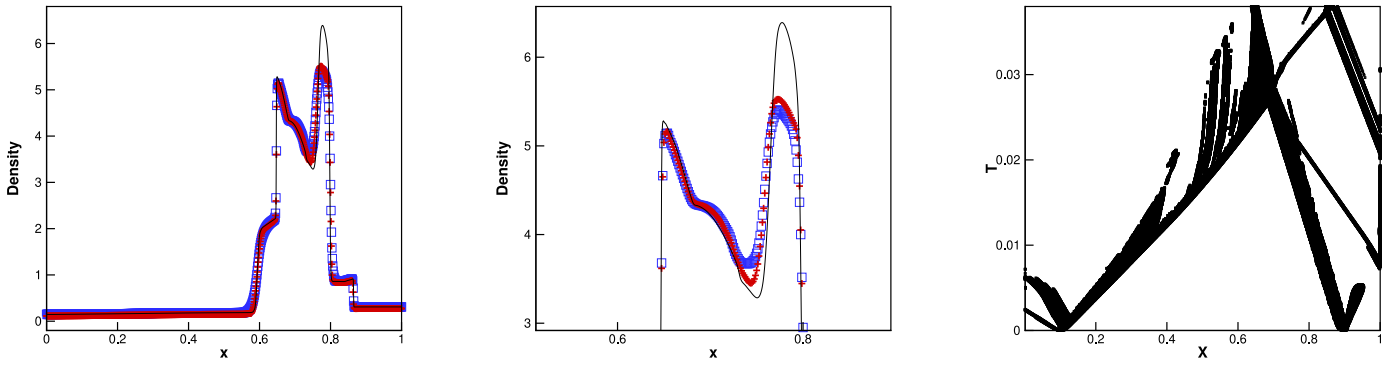

Fig. 3.9. The blast wave problem. T=0.038. From left to right: density; density zoomed in; the points where the simple WENO reconstruction procedure is used in the hybrid WENO scheme. Solid line: the exact solution; plus signs: the results of the hybrid WENO scheme; squares: the results of the simple WENO scheme. Grid points: 800.

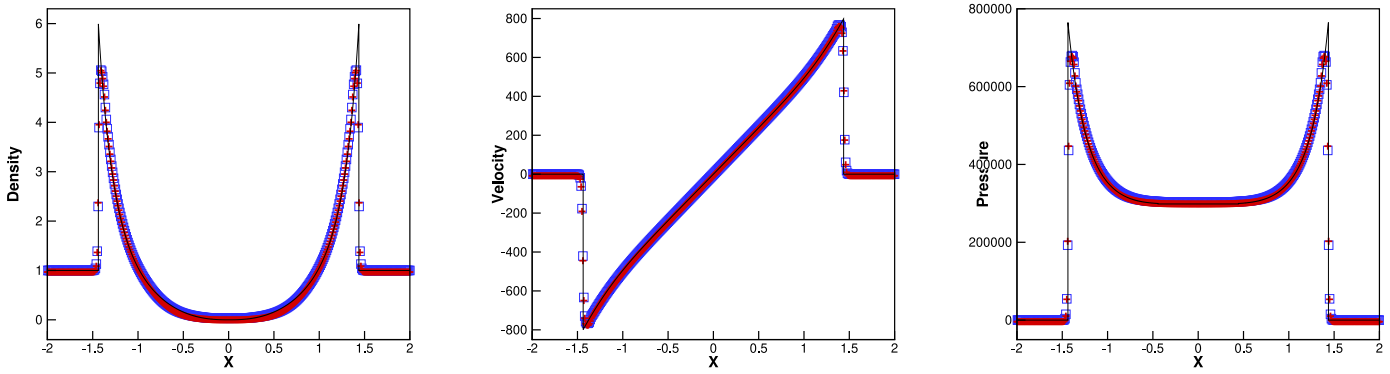

Fig. 3.10. The Sedov blast wave problem. T=0.001. From left to right: density; velocity; pressure. Solid line: the exact solution; plus signs: the results of the hybrid WENO scheme; squares: the results of the simple WENO scheme. Grid points: 400.

the constant $\frac{3200000}{\Delta x}$ in the center cell. The final time is $T = 0.001$. In Fig. 3.10, we present the computational results including the density, velocity and pressure, which are computed by the hybrid WENO scheme and the simple WENO scheme respectively, and the time history of the points where the simple WENO reconstruction procedure is used in the hybrid WENO schemes are illustrated in the left of Fig. 3.13. Likewise, these schemes work well for this extreme test case, while the hybrid WENO scheme saves more than 30% CPU time than the simple WENO scheme given in Table 3.1.

Example 3.7. The double rarefaction wave problem [19]. This test case has the low pressure and low density regions, which is hard to be simulated precisely. The initial conditions are: $(\rho, \mu, p, \gamma)^T = (7, -1, 0.2, 1.4)^T$ for $x \in [-1, 0)$; $(\rho, \mu, p, \gamma)^T = (7, 1, 0.2, 1.4)^T$ for $x \in [0, 1]$. The final computing time is $T = 0.6$. The computational results by the hybrid WENO scheme and the simple WENO scheme including the density, velocity and pressure are shown in Fig. 3.11 and the time history of the points by using the simple WENO reconstruction procedure in the hybrid WENO scheme are illustrated

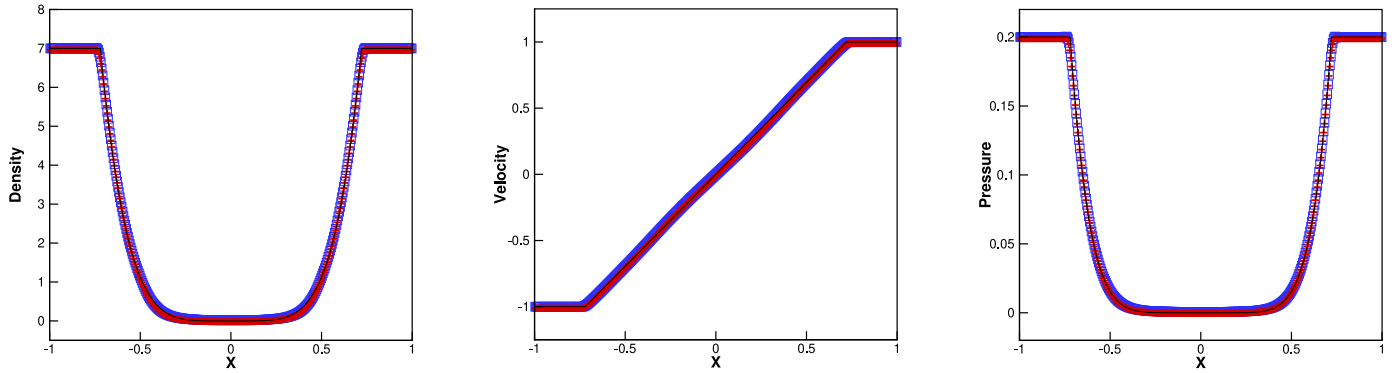

Fig. 3.11. The double rarefaction wave problem. T=0.6. From left to right: density; velocity; pressure. Solid line: the exact solution; plus signs: the results of the hybrid WENO scheme; squares: the results of the simple WENO scheme. Grid points: 400.

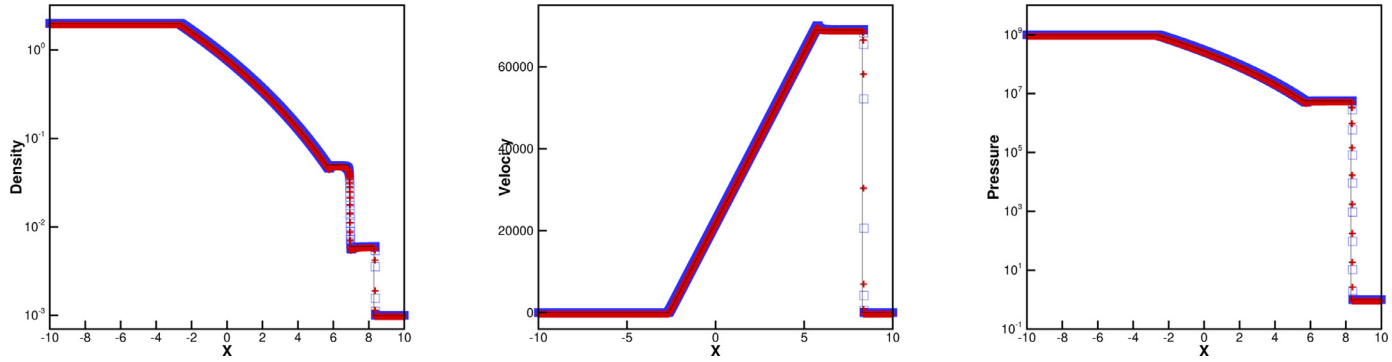

Fig. 3.12. The Leblanc problem. T=0.0001. From left to right: log plot of density; velocity; log plot of pressure. Solid line: the exact solution; plus signs: the results of the hybrid WENO scheme; squares: the results of the simple WENO scheme. Grid points: 6400.

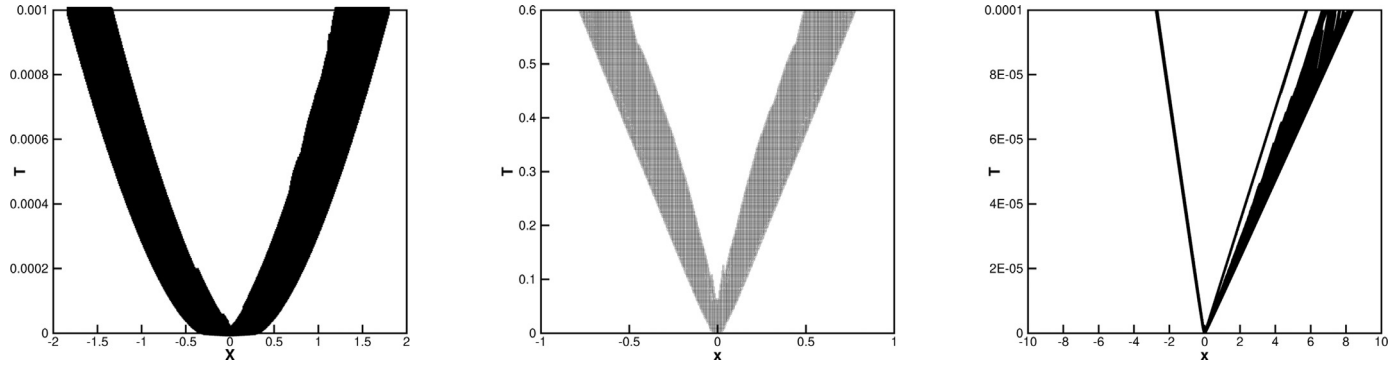

Fig. 3.13. From left to right: the points where the simple WENO reconstruction procedure is used in the hybrid WENO scheme for the Sedov blast wave problem, the double rarefaction wave problem and the Leblanc problem, respectively.

in the middle of Fig. 3.13. We can also see that these two schemes have similar computational results, but the hybrid WENO scheme saves almost 50% CPU time from the Table 3.1.

Example 3.8. The Leblanc problem [19]. The initial conditions are: $(\rho, \mu, p, \gamma)^T = (2, 0, 10^9, 1.4)^T$ for $x \in [-10, 0)$; $(\rho, \mu, p, \gamma)^T = (0.001, 0, 1, 1.4)^T$ for $x \in [0, 10]$. In Fig. 3.12, we present the computational results including the density, velocity and pressure at the final time $T = 0.0001$, which are computed by the hybrid WENO scheme and the simple WENO scheme respectively, and the time history of the points where the simple WENO reconstruction procedure is used in the hybrid WENO schemes are illustrate in the right of Fig. 3.13. Likewise, the computational results by these schemes are similar, and their CPU time are shown in Table 3.1 similarly as the hybrid WENO scheme saves almost 36% computational costs.

Example 3.9. Double Mach reflection problem. We solve the two-dimensional Euler Eqs. (3.2) in a computational domain of $[0, 4] \times [0, 1]$. The reflecting wall lies at the bottom, starting from

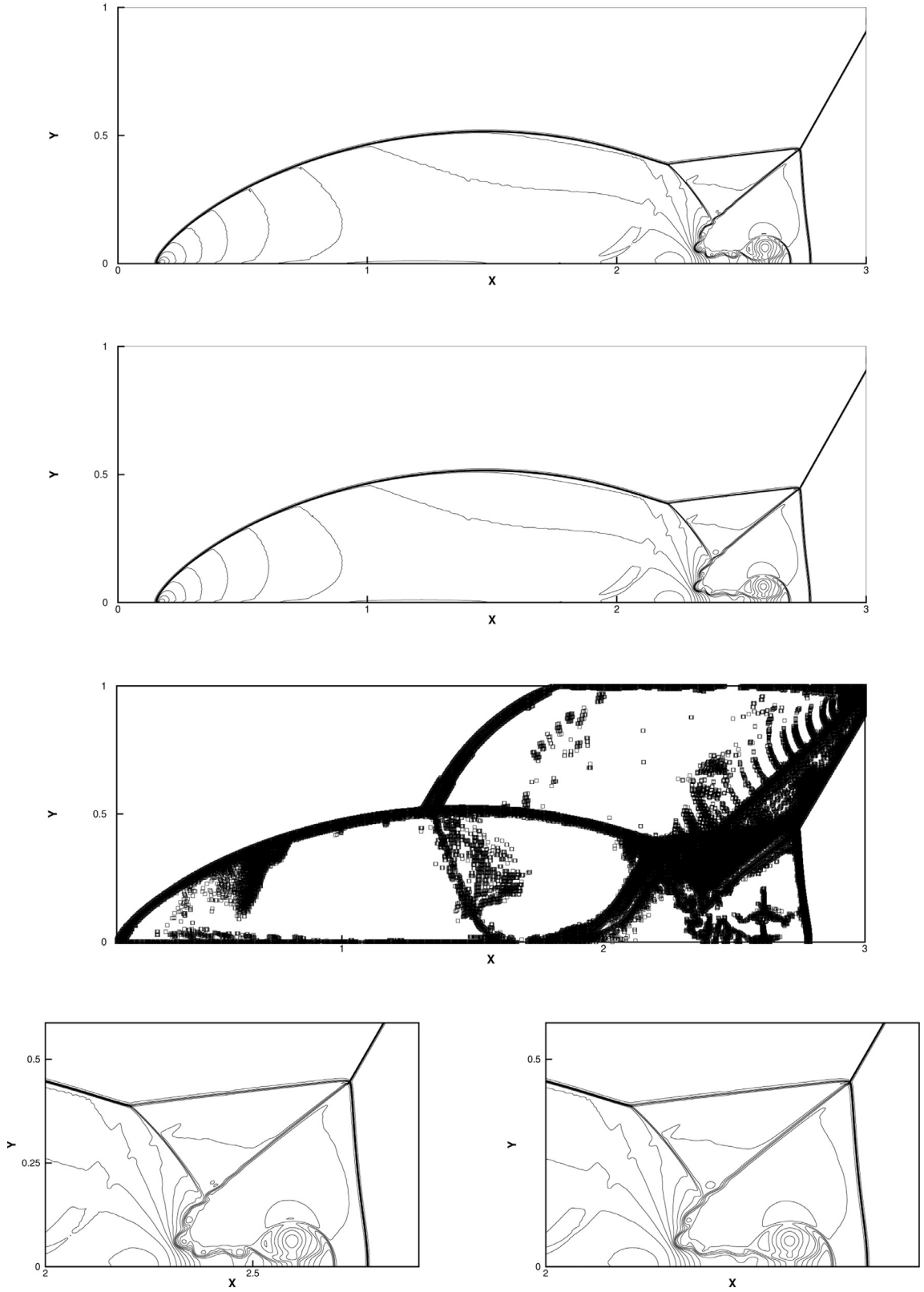

Fig. 3.14. Double Mach reflection problem. T=0.2. 30 equally spaced density contours from 1.5 to 22.7. From top to bottom: the results of the hybrid WENO scheme; the results of the simple WENO scheme; squares denote the points where the simple WENO reconstruction procedure is used in the hybrid WENO scheme; zoomed of the hybrid WENO scheme and the simple WENO scheme. Grid points: 1600 $\times$ 400.

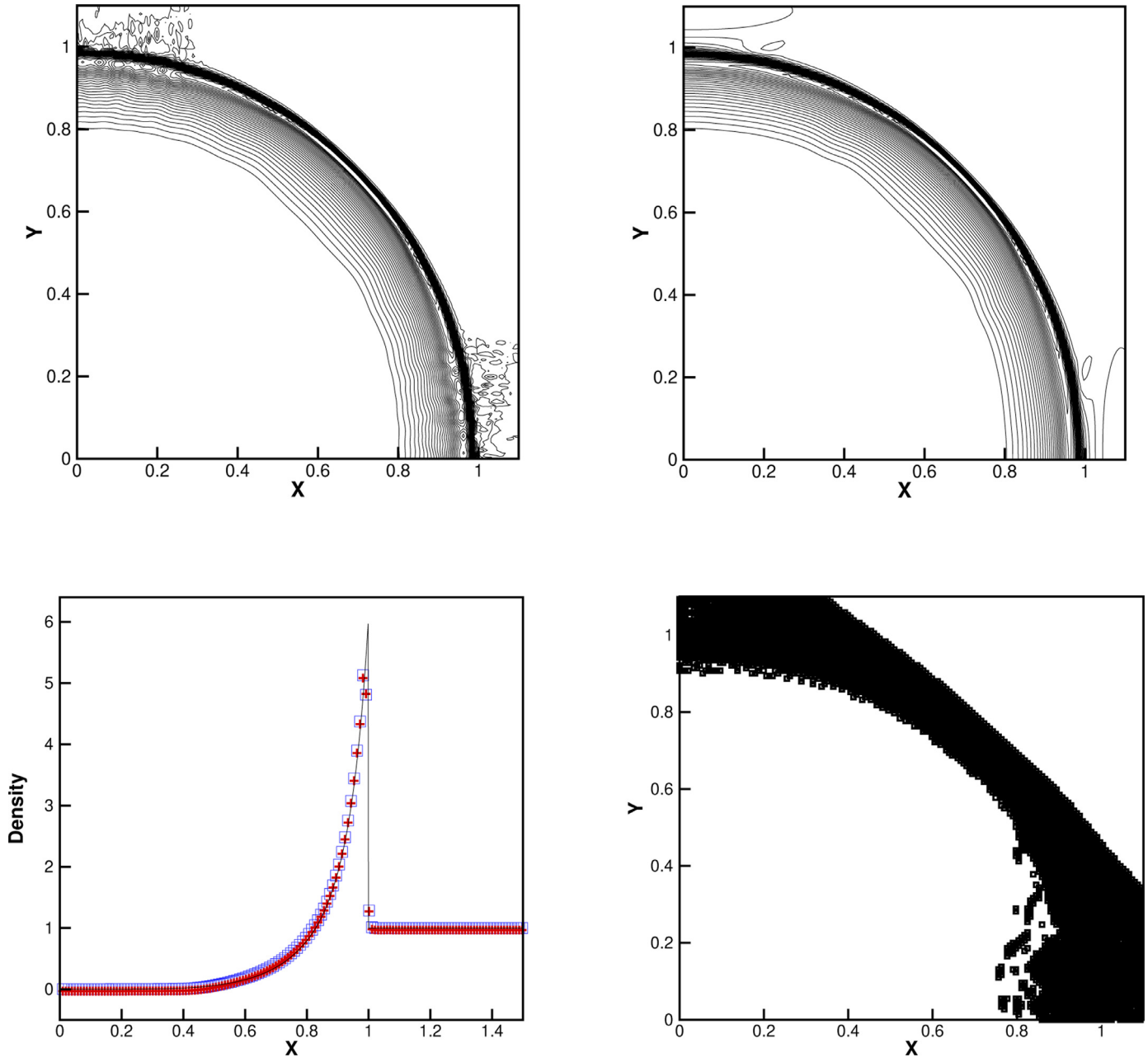

Fig. 3.15. The 2D Sedov problem. T=1. From top to bottom: 30 equally spaced density contours from 0.95 to 5 for two schemes; density is projected to the radical coordinates and the simple WENO reconstruction procedure is used in the hybrid WENO scheme for the 2D Sedov blast wave problem. Solid line: the exact solution; plus signs: the results of the hybrid WENO scheme; squares: the results of the simple WENO scheme. Grid points: 160 × 160.

$x = \frac{1}{6}$, y=0, making a 60^o angle with the x-axis. For the bottom boundary, the exact post-shock condition is imposed for the part from $x = 0$ to $x = \frac{1}{6}$, while the reflection boundary condition is used for the rest. At the top boundary is the exact motion of the Mach 10 shock and $\gamma = 1.4$. The final computing time is $T = 0.2$. We present the results of two schemes in region $[0,\ 3] \times [0,\ 1]$, the points by using the simple WENO reconstruction procedure in the hybrid WENO scheme at the final time and the blow-up region around the double Mach stems in Fig. 3.14. Again, the hybrid WENO scheme and the simple WENO scheme have the same computational results, while the hybrid WENO scheme saves near 25% CPU time shown in Table 3.1.

Example 3.10. The two dimensional Sedov problem [17,23]. The initial conditions are: ρ=1, μ=0, ν=0, $E = 10^{-12}$, $\gamma = 1.4$ everywhere except that the energy is the constant $\frac{0.244816}{\Delta x \Delta y}$ in the lower left corner cell, and the final time is $T = 1$. In Fig. 3.15, we show the computational results by the hybrid WENO and the simple WENO scheme about the density, and the final time of the points where the simple WENO methodology is used in the hybrid WENO scheme are also shown. Again, we can see these two schemes have the same numerical results for this extreme test case, however, the hybrid WENO scheme saves less CPU time illustrated in Table 3.1.

Example 3.11. The high Mach number astrophysical jet problem. For solving the gas and shocks which are discovered by using the

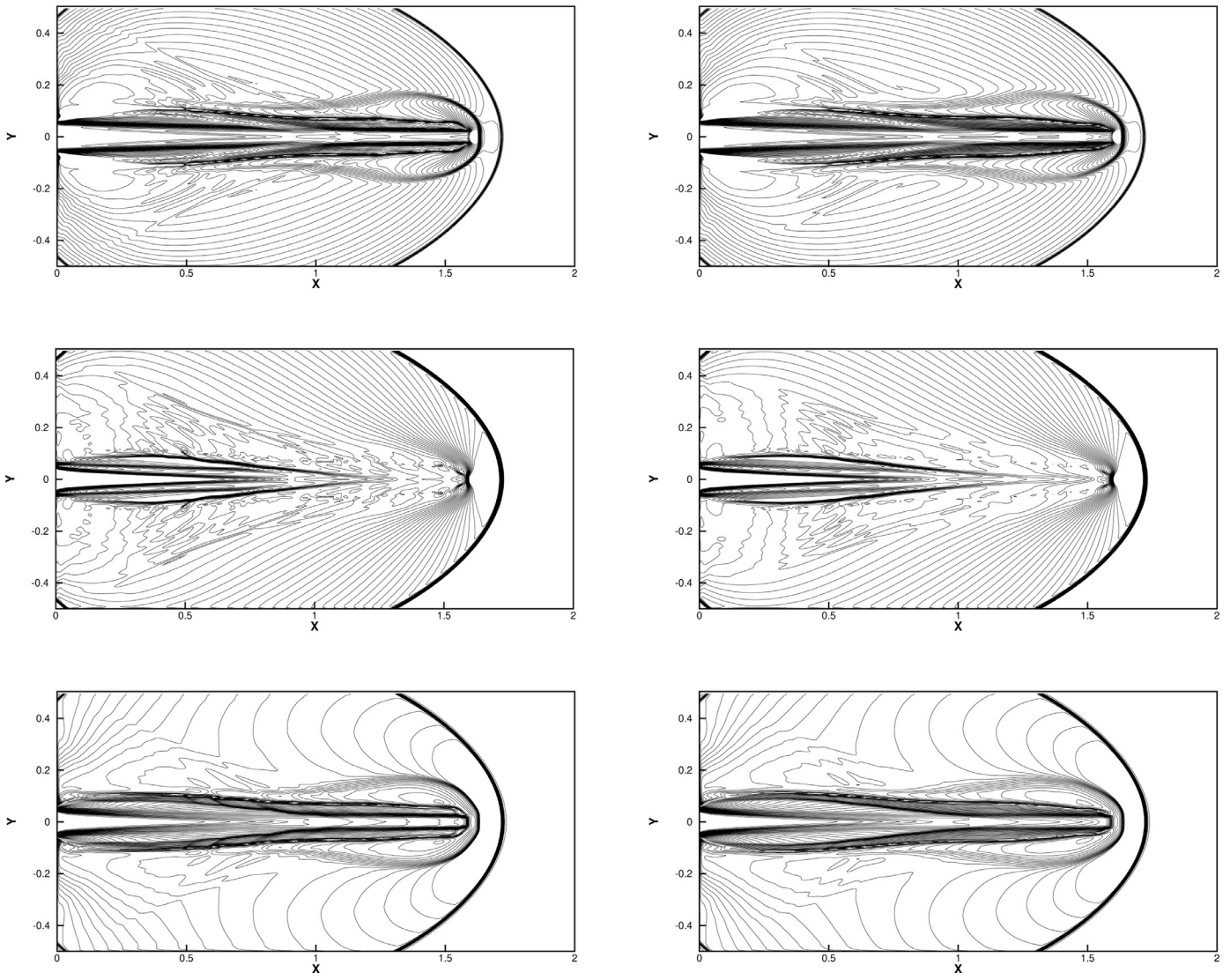

Fig. 3.16. Simulation of Mach 80 jet without radiative cooling problem. T=0.07. Scales are logarithmic. From top to bottom: 40 equally spaced density contours from -2 to 3; 40 equally spaced pressure contours from -0.5 to 5; 40 equally spaced temperature contours from -2 to 4.5. From left to right: Hybrid WENO scheme; Simple WENO scheme. Grid points: 448 × 224.

Hubble space telescope, one can implement theoretical models in a gas dynamics simulator [6,13,14]. A Mach 80 problem (i.e. the Mach number of the jet inflow is Mach 25 with respect to the sound speed in the light ambient gas and Mach 80 with respect to the sound speed in the heavy jet gas) is proposed without the radiative cooling. The initial conditions are: the computational domain is [0,2] × [-0.5,0.5] and is full of the ambient gas with $(\rho, \mu, \nu, p, \gamma)^T = (0.5, 0, 0, 0.4127, 5/3)^T$. The boundary conditions for the right, top and bottom are outflow. For the left boundary $(\rho, \mu, \nu, p, \gamma)^T = (5, 30, 0, 0.4127, 5/3)^T$ for $y \in [-0.05, 0.05]$ and $(\rho, \mu, \nu, p, \gamma)^T = (0.5, 0, 0, 0.4127, 5/3)^T$ otherwise. The final computing time is $T = 0.07$. In Fig. 3.16, we show the numerical results computed by the hybrid WENO scheme and the simple WENO scheme including the density, pressure and temperature, and we also present the final time of the points using the simple WENO reconstruction procedure for the hybrid WENO scheme in the left of Fig. 3.18. The total CPU time of these two schemes is shown in Table 3.1. Then a Mach 2000 problem (i.e. the Mach number of the jet inflow is Mach 25 with respect to the sound speed in the light ambient gas and Mach 2000 with respect to the sound speed in the heavy jet gas) is proposed without the radiative cooling again. The initial conditions are: the computational domain is [0,1] × [-0.25,0.25] and is full of the ambient gas with $(\rho, \mu, \nu, p, \gamma)^T = (0.5, 0, 0, 0.4127, 5/3)^T$. The boundary conditions for the right, top and bottom are outflow. For the left boundary $(\rho, \mu, \nu, p, \gamma)^T = (5, 800, 0, 0.4127, 5/3)^T$ for $y \in [-0.05, 0.05]$ and $(\rho, \mu, \nu, p, \gamma)^T = (0.5, 0, 0, 0.4127, 5/3)^T$ otherwise. We compute this problem till $T = 0.001$. The density, pressure and temperature are shown in Fig. 3.17. The final time of the points using the simple WENO methodology for the hybrid WENO scheme are illustrated in the right of Fig. 3.18. The total CPU time of these two schemes is given in Table 3.1. Likewise, these two schemes work well for this extreme test case, while the hybrid WENO scheme uses less CPU time than the simple WENO scheme.

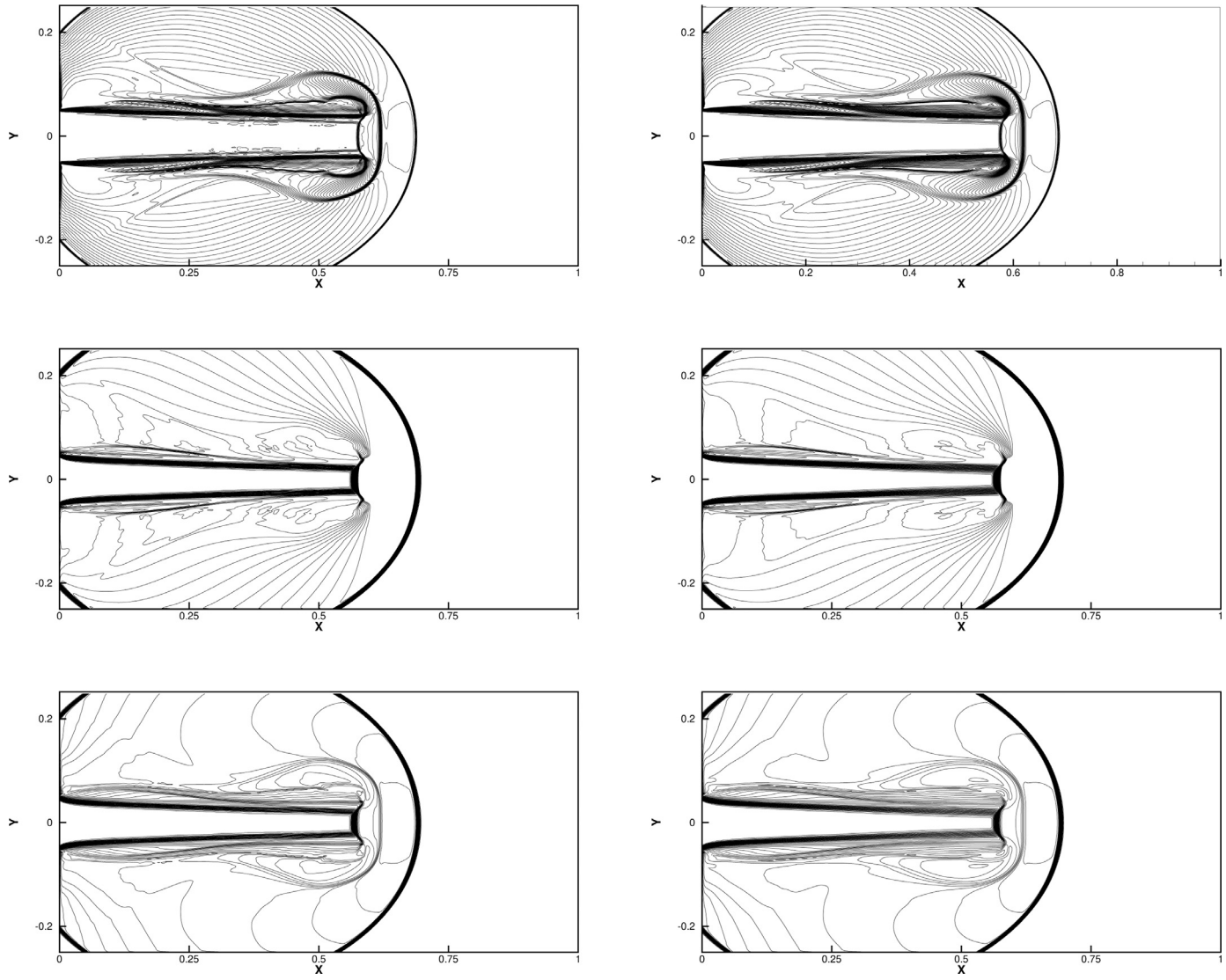

Fig. 3.17. Simulation of Mach 2000 jet without radiative cooling problem. T=0.001. Scales are logarithmic. From top to bottom: 40 equally spaced density contours from -2 to 3; 40 equally spaced pressure contours from -2 to 11; 40 equally spaced temperature contours from -3 to 12.5. From left to right: Hybrid WENO scheme; Simple WENO scheme. Grid points: 640 $\times$ 320.

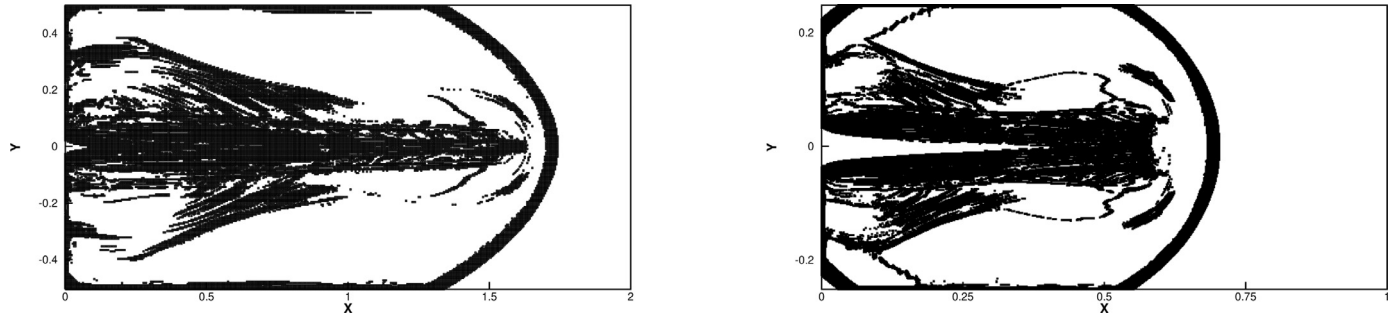

Fig. 3.18. The high Mach number astrophysical jet problem. From left to right: the points where the simple WENO reconstruction procedure is used in the hybrid WENO scheme for the Mach 80 problem and Mach 2000 problem, respectively.

4. Concluding remarks

In this paper, a new type of fifth order accurate finite difference hybrid WENO scheme is designed for solving the hyperbolic conservation laws. Compared with the simple WENO scheme [28], the hybrid WENO scheme is more efficient with less numerical errors in smooth region and less computational costs, and it still keeps the simplicity and robustness of the simple WENO scheme. The hybrid WENO scheme introduced in the previous section and the simple WENO scheme both have the ability to simulate rather extreme test cases such as the Sedov blast wave, the Leblanc and the high Mach number astrophysical jet problems et al. by using a

normal CFL number without any further positivity preserving procedure, while the hybrid WENO scheme uses less CPU time than the simple WENO scheme. In general, these numerical results all illustrate the good performance of the hybrid WENO scheme.

Acknowledgement

The research is partly supported by Science Challenge Project, No. TZ2016002, NSAF grant U1630247 and NSFC grant 11571290.

Appendix A. The steps to solve the cubic equation's real root

In this paper we use the following procedure which is presented in [5] to solve the cubic equation's real root. For arbitrary real coefficient cubic equation $ax^3 + bx^2 + cx + d = 0$, it's real zero points are solved following the steps. Step 1. If $a = 0$, $b = 0$ and $c \neq 0$, the real zero point $x = -d/c$; while $a = 0$, $b = 0$ and $c = 0$, there is no need to solve it's zero point.

Step 2. If $a = 0$ and $b \neq 0$, the cubic equation is reduced to a quadratic equation. If $\Delta = c^2 - 4bd < 0$, the quadratic equation doesn't have real zero point; while $\Delta \geq 0$, it have two real zero point $x_{1,2} = \frac{-c \pm \sqrt{c^2 - 4bd}}{2b}$

Step 3. If $a \neq 0$, we firstly bring in four discriminations, including three multiple root discriminations *A, B, C* and a total discrimination Δ. Their explicit expressions are

$$\begin{cases} A = b^2 - 3ac \\ B = bc - 9ad \\ C = c^2 - 3bd \\ \Delta = B^2 - 4AC \end{cases}$$

1. If $A = 0$ and $B = 0$, the cubic equation has three multiple real roots $x_{1,2,3} = -\frac{b}{3a}$.
2. If $\Delta < 0$, it has three unequal real roots, and the explicit formulas are given as follows,
$$x_1 = \frac{-b - 2\sqrt{A}\cos\frac{\theta}{3}}{3a},$$
$$x_{2,3} = \frac{-b + \sqrt{A}(\cos\frac{\theta}{3} \pm \sqrt{3}\sin\frac{\theta}{3})}{3a},$$
where $\theta = \arccos T$ and $T = (2Ab - 3aB)/(2A^{\frac{3}{2}})$.
3. If $\Delta = 0$, it has three real roots, and one is single root and others are repeated roots. The real roots $x_1 = -b/a + K$ and $x_{2,3} = -K/2$, where K is set as B/A.
4. If $\Delta > 0$, it has one real root and two conjugated imaginary roots, and the explicit expression of the real root x_1 is $-\frac{b + \sqrt[3]{Y_1} + \sqrt[3]{Y_2}}{3a}$, in which $Y_{1,2} = Ab + 3a(\frac{-B \pm \sqrt{B^2 - 4AC}}{2})$, while the formulas of the imaginary roots don't need to be presented here.

References

[1] Borges R, Carmona M, Costa B, Don WS. An improved weighted essentially non-oscillatory scheme for hyperbolic conservation laws. J Comput Phys 2008;227:3191–211.
[2] Casper J. Finite-volume implementation of high-order essentially nonoscillatory schemes in two dimensions. AIAA J 1992;30:2829–35.
[3] Casper J, Atkins HL. A finite-volume high-order ENO scheme for two-dimensional hyperbolic systems. J Comput Phys 1993;106:62–76.
[4] Castro M, Costa B, Don WS. High order weighted essentially non-oscillatory WENO-z schemes for hyperbolic conservation laws. J Comput Phys 2011;230:1766–92.
[5] Fan SJ. A new extracting formula and a new distinguishing means on the one variable cubic equation. J Hainan Norm Univ (NatSci Ed) 1989;2(2):91–8. In Chinese.
[6] Gardner C, Dwyer S. Numerical simulation of the XZ tauri supersonic astrophysical jet. Acta Math Sci 2009;29:1677–83.
[7] Harten A. High resolution schemes for hyperbolic conservation laws. J Comput Phys 1983;49:357–93.
[8] Harten A, Osher S. Uniformly high-order accurate non-oscillatory schemes. IMRC Technical Summary Rept. 2823. WI: Univ. of Wisconsin, Madison, May; 1985.
[9] Harten A. Preliminary results on the extension of ENO schemes to two-dimensional problems. In: Carasso C, et al., editors. Proceedings, International Conference on Nonlinear Hyperbolic Problems, Saint-Etienne. Berlin: Springer-Verlag; 1987. 1986, Lecture Notes in Mathematics.
[10] Harten A, Engquist B, Osher S, Chakravarthy S. Uniformly high order accurate essentially non-oscillatory schemes III. J Comput Phys 1987;71:231–323.
[11] Hu C, Shu CW. Weighted essentially non-oscillatory schemes on triangular meshes. J Comput Phys 1999;150:97–127.
[12] Hill DJ, Pullin DI. Hybrid tuned center-difference-WENO method for large eddy simulations in the presence of strong shocks. J Comput Phys 2004;194:435–50.
[13] Ha Y, Gardner C, Gelb A, Shu CW. Numerical simulation of high mach number astrophysical jets with radiative cooling. J Sci Comput 2005;24:597–612.
[14] Ha Y, Gardner C. Positive scheme numerical simulation of high mach number astrophysical jets. J Sci Comput 2008;34:247–59.
[15] Huang B, Qiu J. Hybrid WENO schemes with lax-wendroff type time discretization. J Math Study 2017;50:242–67.
[16] Jiang G-S, Shu C-W. Efficient implementation of weighted ENO schemes. J Comput Phys 1996;126:202–28.
[17] Korobeinikov V-P. Problems of point-blast theory. 1991. American Institute of Physics.
[18] Liu XD, Osher S, Chan T. Weighted essentially non-oscillatory schemes. J Comput Phys 1994;115:200–12.
[19] Linde T, Roe PL. Robust euler codes, in: 13th computational fluid dynamics conference. AIAA Paper-97-2098.
[20] Li G, Qiu J. Hybrid weighted essentially non-oscillatory schemes with different indicators. J Comput Phys 2010;229:8105–29.
[21] Pirozzoli S. Conservative hybrid compact-WENO schemes for shock-turbulence interaction. J Comput Phys 2002;178:81–117.
[22] Qiu J, Shu CW. A comparison of troubled-cell indicators for runge-kutta discontinuous galerkin methods using weighted essentially nonoscillatory limiters. SIAM J Sci Comput 2005;27:995–1013.
[23] Sedov LI. Similarity and dimensional methods in mechanics. New York: Academic Press; 1959.
[24] Shu C-W, Osher S. Efficient implementation of essentially non-oscillatory shock capturing schemes. J Comput Phys 1988;77:439–71.
[25] Shu CW, Osher S. Efficient implementation of essentially non-oscillatory shock capturing schemes. II, J Comput Phys 1989;83:32–78.
[26] Shu C-W. High order weighted essentially nonoscillatory schemes for convection dominated problems. SIAM Rev 2009;51:82–126.
[27] Zhang YT, Shu C-W. Third order WENO scheme on three dimensional tetrahedral meshes. Commun Comput Phys 2009;5:836–48.
[28] Zhu J, Qiu J. A new fifth order finite difference WENO scheme for solving hyperbolic conservation laws. J Comput Phys 2016;318:110–21.
[29] Zhu J, Qiu J. A new type of modified WENO schemes for solving hyperbolic conservation laws. SIAM J Sci Comput 2017;39:A1089–113.
[30] Zhu J, Qiu J. A new type of finite volume WENO schemes for hyperbolic conservation laws. J Sci Comput 2017;73:1338–59.
[31] Zhu J, Qiu J. A new third order finite volume weighted essentially non-oscillatory scheme on tetrahedral meshes. J Comput Phys 2017;349:220–32.
[32] Zhu J, Qiu J. A simple finite volume weighted essentially non-oscillatory schemes on triangular meshes. SIAM J Sci Comput 2018;40:A903–28.